Available online at www.sciencedirect.com
SCIENCE DIRECT®
Journal of Structural Biology 141 (2003) 171–178
Journal of Structural Biology
www.elsevier.com/locate/yjsbi

Crystallization Note

Crystal structure of pokeweed antiviral protein with well-defined sugars from seeds at 1.8 Å resolution

Zong-Hao Zeng,[a] Xiao-Lin He,[a] Hong-Min Li,[a] Zhong Hu,[b] and Da-Cheng Wang[a,c,*]

[a] *Center for Molecular Biology, Institute of Biophysics, Chinese Academy of Sciences, Beijing 100101, China*
[b] *Kunming Institute of Botany, Chinese Academy of Sciences, Kunming 650204, China*
[c] *National Laboratory of Microgravity, Chinese Academy of Sciences, Beijing, China*

Received 26 December 2001, and in revised form 18 October 2002

Abstract

The crystal structure of pokeweed antiviral protein from seeds of *Phytolacca americana* (PAP-S) was solved at 1.8 Å. PAP-S is a one-chain ribosome-inactivating protein (RIP) and distinctively contains three well-defined *N*-acetylglucosamines, each covalently linked to an asparagine residue at positions, 10, 44, and 255, respectively. The high-resolution structure clearly shows the three mono-sugars to have either an α- or a β-conformation. Two of sugars are located on the same side of the molecule with the active pocket. Except one hydrogen bond, there are no intermolecular interactions between the polypeptide chain and the sugars. Instead the sugar conformations appear to be stabilized by intermolecular interactions. The sugar structure defined at high resolution provides a structural basis for understanding their possible biological activity. The structural comparisons of PAP-S with other PAPs reveal that the major disparity of these homologous molecules is the different charge distribution on the upper right side of the front side near the active pocket. Based on the available structure of the 50S ribosomal subunit, the possible interactions between PAPs and the ribosome are discussed.

Keywords: Pokeweed antiviral protein; Ribosome-inactivating protein; *N*-Acetylglucosamine; Crystal structure

1. Introduction

Pokeweed antiviral proteins (PAPs)[1] are members of the type I ribosome inactivating proteins (RIPs). Many plants produce different RIPs, which can catalytically inactivate ribosome and thereby inhibit protein synthesis (Barbieri et al., 1993; Stirpe et al., 1992). As is well known, most of the RIPs consist of one or two peptide chains, and are, respectively, classified as type I or type II RIPs. The type I RIPs are similar in sequence, and even more in structure, to the active chain of the type II RIPs, such as the ricin A-chain. All RIPs are RNA *N*-glycosidases. They are characterized by their ability to cleave the *N*-glycosidic bond of a specific exposed adenine base on the sarcin-ricin-loop (SRL) of the large rRNA subunit (Endo et al., 1991). This loop is responsible for the binding of the elongation factor to the ribosome (Correll et al., 1998). Depurination of the SRL impairs the binding interaction between SRL and elongation factor, resulting in irreversible inhibition of protein synthesis.

Many RIPs are discovered by their ability to inhibit the growth of microbes, such as viruses, bacteria, and fungi. It had been believed that their antimicrobial activity is based on their *N*-glycosidase activity at the specific site of SRL. Crystal structures revealed that the active pocket and some catalytic mechanisms were also proposed (Huang et al., 1995; Monzingo and Robertus, 1992). Recent experiments showed that RIPs can depurinate adenine in DNA, rRNA, and poly(A) with a wide range of activity and specificity, and act as nucleases cleaving DNA (Barbieri et al., 1997). But how they work on these substrates is still unclear (Wang et al., 1999).

* Corresponding author. Fax: +86-10-64888560.
E-mail address: dcwang@sun5.ibp.ac.cn (D.-C. Wang).

[1] *Abbreviations used:* RIPs, ribosome-inactivating proteins; PAPs, pokeweed antiviral proteins; PAP, pokeweed antiviral protein from leaves; α-PAP, pokeweed antiviral protein from genomic clones; PAP-S, pokeweed antiviral protein from seeds; SRL, sarcin-ricin-loop.

1047-8477/02/$ - see front matter © 2002 Elsevier Science (USA). All rights reserved.
doi:10.1016/S1047-8477(02)00580-4

PAPs are also discovered by their ability to inhibit the proliferation of viruses (Barbieri et al., 1982; Irvin et al., 1980; Irvin, 1975). Now, we know that at various developing stages the different tissues of the plant, *P. americana* (pokeweed), synthesize different PAPs. PAP-I was found from spring leaves (Irvin, 1975), PAP-II from summer leaves (Irvin et al., 1980), PAP-S from seeds (Barbieri et al., 1982), and PAP-R from roots (Bolognesi et al., 1990). Other isozymes are also found in cell culture (PAP-C), or resulted from genomic clones (α-PAP) (Kataoka et al., 1992). Most recently two isoforms, PAP-S1 and S2, from seeds were identified (Honjo et al., 2002). Sequence alignment showed that PAP-S reported in this paper corresponded to PAP-S1.

Crystal structures of PAP-I, α-PAP, and PAP-II have been determined at different resolutions (Ago et al., 1994; Kurinov et al., 1999a, b; Monzingo et al., 1993). What makes PAP-S different from other PAPs are the three *N*-acetylglucosamines, each covalently connected to one of the three asparagines at site 10, 42, and 255, respectively (Islam et al., 1991). In biological activity, PAP-S and α-PAP are toxic to eukaryotic cells only, whereas PAP-I is toxic to both eukaryotic and prokaryotic cells.

Here we report the crystal structure determination of PAP-S (S1, Honjo et al., 2002)[2] at 1.8 Å resolution and a structural comparison between PAP-S and other RIPs. The well-defined sugar structure is visible at high resolution. A recent report shows that the ribosomal protein L3 is required for PAP-I to access ribosomes (Hudak et al., 1999). This is the first experimental evidence that the interaction between RIP and ribosome protein is necessary for the in vivo effects of RIPs. The latest structural analysis of a 50S ribosome subunit placed the constituent proteins and RNA structures into a 2.4 Å resolution map (Ban et al., 1999, 2000). On this basis, possible interactions between PAP-S and the ribosome are discussed.

2. Materials and methods

2.1. Sample and crystallization

A sample of PAP-S was purified from seeds of *P. americana*. The crystals were grown under high temperature (33 °C) and high protein concentration (100 mg/ml) in about 50 days. Both procedures for protein purification and crystallization were described in preliminary reports (Li et al., 1998; Zhu and Hu, 1989).

The crystal belongs to space group I222 with cell parameters $a = 84.76$ Å, $b = 78.05$ Å, and $c = 91.57$ Å. The crystal contains one molecule per asymmetric unit and the solvent content is estimated to be approximately 53%.

[2] The paper appeared after this manuscript was submitted.

2.2. Data collection and processing

The diffraction data were collected from one crystal on the beam line BL6A2 of the Photon Factory in KEK, Trukuba of Japan, at room temperature with wavelength 1.0 Å, by using a screenless Weissenburg Camera and Image Plates (Sakabe, 1989). The data were evaluated, scaled, and merged with the program WEIS (Higashi, 1989). In order to improve the completeness a data set at 2.2 Å resolution was collected on a MAR 340 image plate detector with CuKα radiation ($\lambda = 1.5418$ Å) from an in-house X-ray generator operating at 40 kV and 50 mA, and then combined with the data from the synchrotron station using the Scalpack program in the HKL package (Otwinowski and Minor, 1997) with an R_{merge} of 9.6%. The final statistics on data collection are listed in Table 3.

2.3. Molecular replacement

The structure of PAP-S was solved by the molecular replacement method using AMoRe (Navaza, 1994). The crystal structure of PAP-I (PDB ID Code 1pdf) was used as a search model. No atom was substituted or omitted from the model. Patterson cutoff radius is 25 Å. Data in the 20–4.0 Å resolution range were used. The "rotting" run gave a peak with correlation coefficient (CC) 19.1%, twice that of the second. The "training" run raised the CC to 51.2% and gave an *R* factor of 41.5%. The "fitting" run raised the CC to 59.6% and reduced the *R* factor to 38.6%. This unambiguous solution from molecular replacement was conformed by a check of packing with TURBO-FRODO (Roussel and Cambillau, 1991).

2.4. Model building and refinement

The model was rebuilt using the TURBO-FRODO (Roussel and Cambillau, 1991) and O (Jones et al., 1991), and was refined firstly at 2.5 Å and then at 1.8 Å resolution with X-PLOR (Brünger et al., 1987). No data truncation was applied in the refinement, as suggested by Dodson et al. (1996). Ten percent of the data was set aside in order to calculate the free *R* factor (Kleywegt and Brünger, 1996). Most water molecules were located automatically by water picking with X-PLOR. Crystallographic and geometric statistics for the final model are listed in Table 1. The refined final model of PAP-S includes 2053 protein atoms and 499 water molecules, three *N*-acetylglucosamine groups were modeled in $(2F_o - F_c)$ and $(F_o - F_c)$ maps with definite density and reasonable stereochemistry. The final structure was validated using the program PROCHECK (Laskowski et al., 1993). The Ramachandran plot (Ramachandran and Sasusekharan, 1968) reveals that all residues are in allowed regions (Table 3).

Table 1
Hydrogen bonds between *N*-acetylglucosamines protein

Sugar atom	Protein atom	Distance
NAG1 O6	Lys^{15} NZ	2.95
NAG1 O8	#Glu^{227} OE2	2.75
NAG3 O4	#Thr^{212} OG1	2.37
NAG3 O6	#Tyr^{253} O	2.77

Symmetry-related molecules in the crystal.

2.5. Accession Number

Coordinates of PAP-S have been deposited in the Protein Data Bank with PDB ID 1GIK and SCSB ID RCSB001555.

3. Results and discussion

3.1. General structure

The molecule contains eight β-strands (b1–b8) and nine α-helices (h1–h9) (Fig. 1). Previously, for α-PAP, it was divided into three domains (Ago et al., 1994). Here we prefer a division of two domains, which assigned the first two helices and the first six strands as the first domain, and others as the second domain (Fig. 1). The active pocket is just at the intersection of the domain interface and the horizontal groove under the ridge formed by the two loops, respectively, connecting to the two N-ends of h2 (13–27) and h3 (95–105) (Fig. 1B). If we look right into the active pocket, the part of the molecular surface just in front of our eyes is denoted as the front face, whereas the other part will be called the back face. The active pocket is right in the center of the front face. (Fig. 1B)

The three mono-sugars are attached to the PAP-S molecule with definite conformations. They all protrude from the molecular surface (Fig. 1A). In this paper, the three *N*-acetylglucosamine connected to Asn^{10}, Asn^{44}, and Asn^{255} are denoted by NAG1, NAG2, and NAG3, respectively. Among others, NAG1 is situated just at the tight turn connecting the first β-strand (b1) to the first α-helix (h1). Generally speaking, the three mono-saccharides protruding from the molecular surface cannot have extensive interactions with the peptide part of the protein. Therefore these sugar residues may play a role mainly in intermolecular interactions such as molecular recognition or adhesion. The observation here in PAP-S is similar to that from other glycoproteins (Wormald and Dwek, 1999).

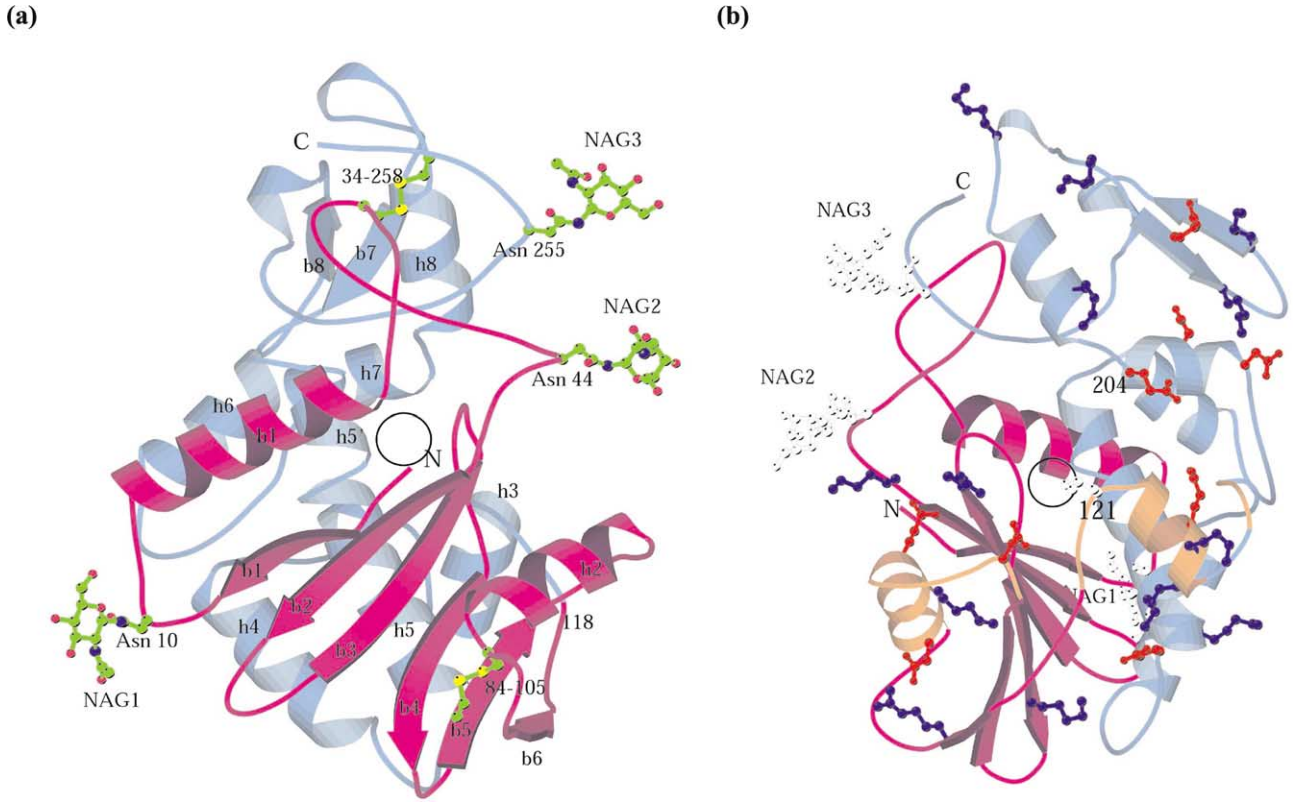

Fig. 1. General structure of PAP-S. (A) Side view of the overall structure of PAP-S. The two domains are differentiated by colors. The circle denotes the position of the active pocket. NAG1, NAG2, and NAG3 are the three acetylglucosamines. (B) Front view of the PAP-S. The two domains are in different colors. The three loops constitute the ridge of the groove, as well as the two helices (h2 and h3) with their N-end rise out from the ridge, and are colored in orange. The active pocket (circle) is at the intersection between the groove and the domain interface. The positive and negative residues on the front surface are in blue and red, respectively. The figures were drawn with MOLSCRIPT (Kraulis, 1991).

3.2. Structure of three N-acetylglucosamines

All three mono-sugars fit to electron density maps very well as shown in Fig. 2. They are mainly stabilized by intermolecular contacts from crystal packing. In NAG1 there are two hydrogen bonds formed between NAG1 O6 and NE of residue Lys^{15} on the end of h1, as well as NAG1 O8 and OE2 of the symmetry-related residue Glu^{227}. Both hydrogen bonds appeared in NAG3 and are formed between the sugar and the neighboring molecules (Table 2 and Fig. 2). These interactions give NAG1 and NAG3 fine structures on the molecular surface of PAP-S. For NAG2, though no hydrogen bonds, the nonbonded interactions (e.g., NAG2 O4... #Arg^{67} NH1, 3.79 Å) from crystal packing define its structure, which is rather looser than NAG1 and NAG3 (Fig. 2B).

The three hex-atomic rings of the three *N*-acetylglucosamines adopt a chair conformation. But the chair of NAG2 is different from the chairs of NAG1 and NAG3, as indicated by the torsion angles of C1–C2–C3–C4 (Table 2) and the electronic density (Fig. 2B). The chirality at atoms C2, C3, C4, and C5 is the same for the three sugars, but at atom C1, NAG2 has a different chirality from the other two. This difference in chirality puts NAG2 in α conformation whereas NAG1 and NAG3 are in β conformation. The three sugar rings are able to rotate somewhat around the Nδ2–C1 bond to find a more suitable conformation as reflected in the torsion angles CG–ND2–C1–C2 (Table 2).

3.3. Comparison with other PAPs

The general structure comparison by superimposed α-carbon and the sequence alignment by structure for PAP-S, α-PAP, and PAP-I is shown in Figs. 3A and B,

Table 2
Conformations of the three *N*-acetylglucosamines

Torsion angle	NAG1	NAG2	NAG3
CG–ND2–C1–C2	102.82	−101.12	61.57
C1–C2–C3–C4	−48.19	57.69	−52.02

Table 3
Data collection and structural refinement statistics

(A) *Data collection*	
Raw data	68617
Unique	23204
Resolution (Å)	1.8
R_{merge} (%)	6.2 (29.6)[a]
Completeness (%)	82.0 (69.5)[a]
$I/\sigma(I)$	16.8 (8.5)
(B) *Structural refinement*	
Resolution range	20.0–1.80
Number of reflections($F > 0$)	23,204
R Factor	0.198 (0.288)[a]
Free *R*	0.242 (0.294)[a]
Number of non-hydrogen atoms	2597
Protein	2053
N-Acetylglucosamine	45
Water	499
Averaged *B* factors (Å^2)	28.9
Main chain	25.5
Side chain	25.7
N-Acetylglucosamine	34.0
Water	41.1
Deviation from standard geometry	
Bond length (Å)	0.010
Bond angle (°)	1.698
Distribution of Ramachandran angles (%)	
Most favored	84.0
Additionally allowed	15.6
Generously allowed	0.4

[a] Data in the outmost shell, 1.88–1.80 Å.

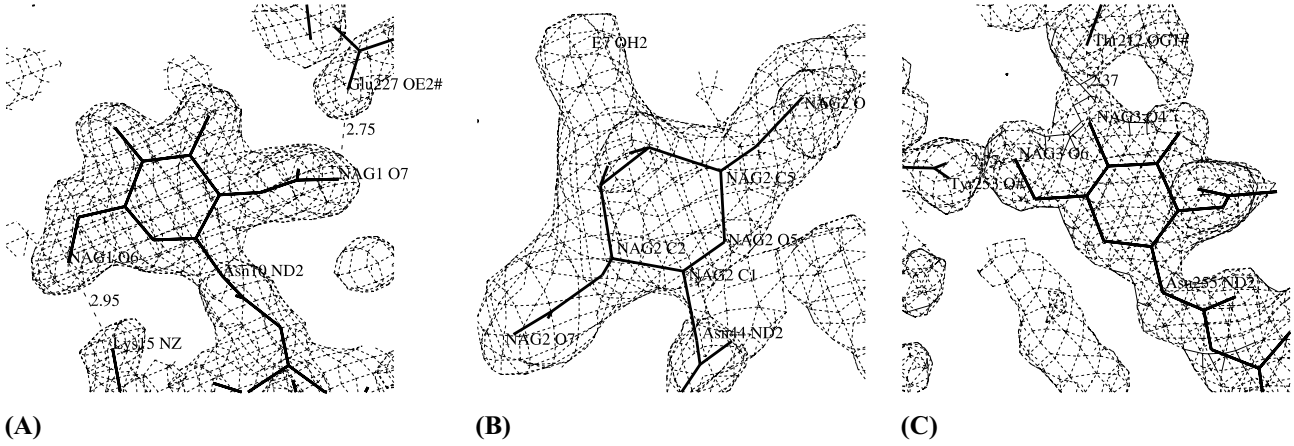

Fig. 2. The $2F_o - F_c$ electron density maps of the three *N*-acetylglucosamines contoured at 1σ. All of them are oriented with the hydrogen atom on each C1 toward the reader. Hydrogen bonds are denoted by dashed lines with numbers denoting the respective distances in unit of Å. # denotes atoms from a symmetry-related molecule. Figures were drawn with O (Jones et al., 1991).

(a)

(b)

```
                  1         2         3         4         5         6
PAP-S     INTITFDAGNATINKYATFMESLRNEAKDPSLKCYGIPMLPNTNSTIKYLLVKLQGASLKTI
PAP       VNTIIYNVGSTTISKYATFLNDLRNEAKDPSLKCYGIPMLPNTNTNPKYVLVELQGSNKKTI
α-PAP     INTITFDVGNATINKYATFMKSIHNQAKDPTLKCYGIPMLPNTNLTPKYLLVTLQDSSLKTI
              B1            H1                                  B2
                 7         8          9         10        11         12
PAP-S     TLMLRRNNLYVMGYSDPYDN-KCRYHIFNDIK-GTEYSDVENTLCPSSNPRVAKPINYNGLY
PAP       TLMLRRNNLYVMGYSDPFETNKCRYHIFNDIS-GTERQDVETTLCPNANSRVSKNINFDSRY
α-PAP     TLMLKRNNLYVMGYADTYNG-KCRYHIFKDISNTTERNDVMTTLCPNPSSRVGKNINYDSSY
            B3         B4          B5            H2            B6
                13        14        15        16        17        18
PAP-S     PTLEKKAGVTSRNEVQLGIQILSSDIGKISGQGSFTEKIEAKFLLVAIQMVSEAARFKYI
PAP       PTLESKAGVKSRSQVQLGIQILDSNIGKISGVMSFTEKTEAEFLLVAIQMVSEAARFKYI
α-PAP     PALEKKVGR-PRSQVQLGIQILNSGIGKIYGVDSFTEKTEAEFLLVAIQMVSEAARFKYI
            H3                  H4                  H5        H5'
                19        20        21        22        23        24
PAP-S     ENQVKTNFNRDFSPNDKVLDLEENWGKISTAIHNSKNGALPKPLELKNADGTKWIVLRVD
PAP       ENQVKTNFNRAFNPNPKVLNLQETWGKISTAIHDAKNGVLPKPLELVDASGAKWIVLRVD
α-PAP     ENQVKTNFNRAFYPNAKVLNLEESWGKISTAIHNAKNGALTSPLELKNANGSKWIVLRVD
            H6                  H7        H8          B7            B8
                25        26
PAP-S     EIKPDVGLLNYVNGTCQAT
PAP       EIKPDVALLNYVGGSCQTT
α-PAP     DIEPDVGLLKYVNGTCQAT
```

Fig. 3. Comparisons of PAPs. (A) Stereo view of the superimposed α-carbons of PAP-S (broken line) with PAP-I (solid line) and α-PAP (dotted line). The arrow indicates the loop with the highest structural diversity. (B) Sequence alignment by structure. Residues in α-helices and β-strand are, respectively, underlined by wavy and straight lines. Secondary structures are calculated by use of PROCHECK (Laskowski et al., 1993).

respectively. Sequence similarities among these three PAPs with known three- dimensional structures are about 75–80%. Aligned by structure, there are two sites where insertions, or deletions, occur. From 80 to 83 (at the bottom middle in Fig. 3A), the three sequences, respectively, are YDN-K for PAP-S, FETNK for PAP-I, and YNG-K for α-PAP (Fig. 3B). From 92 to 95 (indicated by the arrow in Fig. 3A), the three sequences, respectively, are IK-GT for PAP-S, IS-GT for PAP-I, and ISNTT for α-PAP. From 130 to 133 (at the bottom left in Fig. 3A), the three sequences, respectively, are GVTSR for PAP-S, GVKSR for PAP-I, and GR-PR for α-PAP (Fig. 3B). For the structurally well-aligned 251 residues (PAP-S has 261 residues), the root mean square deviations are below 0.82 Å for main-chain atoms and 1.44 Å for side-chain atoms, respectively. The most

conserved region is at the active pocket (the central part displayed in Fig. 3A) in both structure and sequence. These indicate that the enzymatic mechanism is essentially the same for the three isozymes as proposed previously (Monzingo and Robertus, 1992).

In the reported structures of momordin and α-momorcharin (1mom, 1mrg, and 1mrh), the Ramachandran angles of the residue Asp^{77} are in the disallowed region. The sequence of momordin at 76–79 reads as ADTT which adopt a tight turn structure. These residues structurally align to residues 80–83 of PAP-S. The residue Asp^{81} in PAP-S, corresponding to Asp^{77} in momordin, has the Ramachandran angles falling in the favorite region. In PAP-S, the nitrogen atom on Lys^{83} interacts with the oxygen atom on the peptide bond between 81 and 82. This makes the peptide bond flip 180° and changes the Ramachandran angle of Asp^{81}. Observation of the structures of α-momorcharin suggests that interactions of the two oxygen atoms on residue Asp^{77} with the two nitrogen atoms, respectively, on the two peptide bonds related to residue 77 stabilize the unusual Ramachandran angle. However, there is a residue, Gln219, in a turn of PAP-S falling into the generously allowed region of the Ramachandran plot. The well-defined densities prove these observations.

The structurally most diverse region is the loop connecting b5 to h2 (Fig. 3A). It is part of the ridge beside the groove, and at the entrance of the active pocket. The main characteristics that make PAPs different from each other is charge distributions, or electron-static potentials (Fig. 4). At the upper-right part, PAP-S is more negative. It has four negative residues there (see Fig. 1B), whereas PAP-I and α-PAP have only two. Besides, there is a positive residue, Arg^{122}, near the entrance of the active pocket of PAP-I, whereas the equivalent residue in PAP-S is Leu^{121}. This positive residue causes a disruption of the negative charge strip on the horizontal ridge, making the electronic characteristics of PAP-I at the entrance of the active pocket different from those in PAP-S and α-PAP. Furthermore, the negative residue Glu^{204} in PAP-S is mutated to Gln^{205} in PAP-I and α-PAP (Fig. 3B).

3.4. Possible interactions with ribosome

It is well known that PAP-S as the type I ribosome-inactivating protein are characterized by their ability to cleave the *N*-glycoside bond of a specific adenine base exposed on the SRL of the large rRNA subunit (Endo et al., 1991). But the interactions between PAPs and the ribosome are still unclear. Most recently structural analysis of the 50S ribosome subunit has placed the constituent proteins and RNA structures into a 2.4 Å resolution map (Ban et al., 1999, 2000). This structure model (the coordinates were taken from Protein Data Bank 1c04 and 1ffk) showed that the SRL is buried in the 50S ribosome subunit with the tetra-loop GAGA at the surface, allowing EF-G to bond. PAPs have many opportunities to contact other proteins in the ribosome. A recent report experimentally confirmed that, for PAP to access ribosome and cleave the purine ring, the ribosome protein L3 is required (Hudak et al., 1999). This experimental evidence showed the possible interactions between a RIP and the ribosome. However, checking the structural model of the 50S ribosome subunit showed that the protein L3 is at the opposite end of the SRL opposed to the tetra-loop GAGA, and has a distance at least 35 Å away from the tetra-loop of SRL. This makes

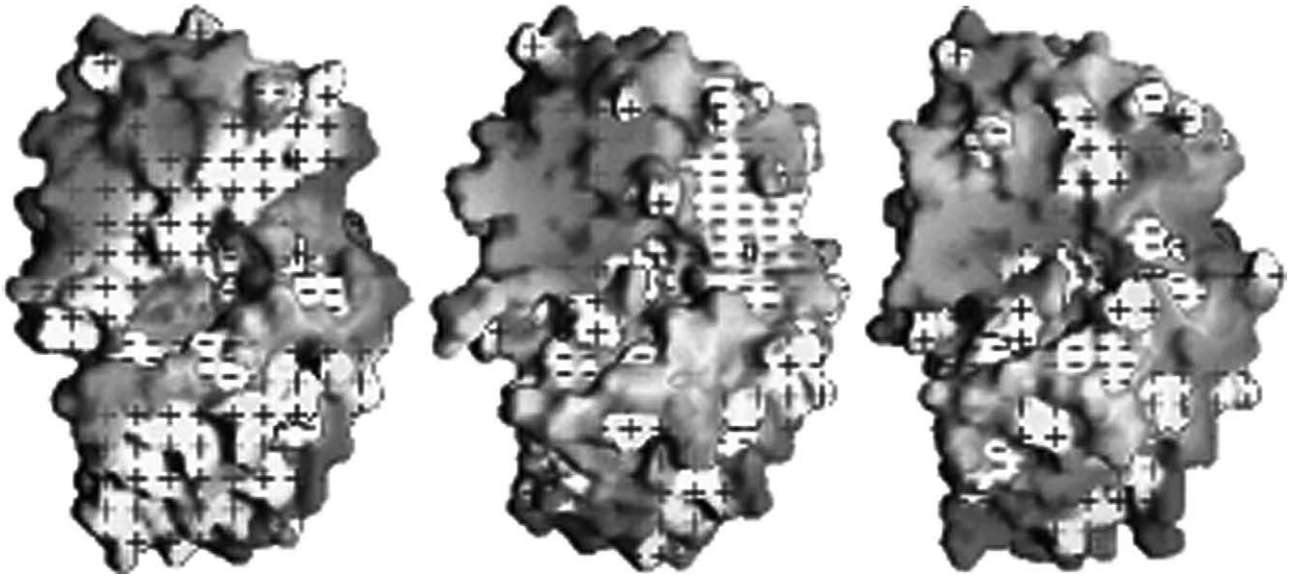

Fig. 4. The molecular surface of α-PAP (left), PAP-S, and PAP-I (right). The positive and negative charge potential are highlighted by "+" and "–," respectively. The orientation of the molecules is the same as that in Fig. 1B. Figures were drawn with GRASP (Nicholls, 1991).

PAPs and any RIPs unable to reach L3 at the same time they are processing the tetra-loop. The biochemical data and the structural consideration suggest a multiple-step process for the inactivation of ribosome by PAPs, binding to L3 and then processing the tetra-loop. Another possibility is that the PAPs may interact with the disintegrated ribosome. More experiment evidence is required for clarification.

As the active pocket is deeply under the molecule's front face (Fig. 1B), when PAP-S is approaching the tetra-loop on SRL, the molecule's front face has the potential of touching the ribosome. Some residues on this surface, including two sugars, NAG2 and NAG3, protruding from this surface (Fig. 1B), may be involved in the possible interactions with the 50S ribosome subunit.

Acknowledgments

This project was supported by the National Basic Research Program (G19990756, 95-yu-34), NNSF (Grant 30070162) of China, and the Chinese Academy of Sciences. The X-ray data collection was supported by the Photon Factory of KEK, Japan. We are grateful to Drs. N. and K. Sakabe for their kind help in data collection.

References

Ago, H., Kataoka, J., Tsuge, H., Habuka, N., Inagaki, E., Noma, M., Miyano, M., 1994. X-ray structure of a pokeweed antiviral protein, coded by a new genomic clone, at 0.23 nm resolution. Eur. J. Biochem. 225, 369–374.

Ban, N., Nissen, P., Hansen, J., Capel, M., Moore, P.B., Steitz, T.A., 1999. Placement of protein and RNA structures into a 5 Å resolution map of the 50S ribosome subunit. Nature 400, 841–847.

Ban, N., Nissen, P., Hansen, J., Moor, P.B., Steitz, T.A., 2000. The complete atomic structure of the large ribosomal subunit at 2.4 Å resolution. Science 289, 905–919.

Barbieri, L., Aron, G.M., Irvin, J.D., Stirpe, F., 1982. Purification and partial characterization of another form of the antiviral protein from the seeds of *Phytolacca americana* L (pokeweed). Biochem. J. 203, 55–59.

Barbieri, L., Battelli, M.G., Stirp, F., 1993. Ribosome-inactivating proteins from plants. Biochim. Biophys. Acta 1154, 237–282.

Barbieri, L., Valbonesi, P., Bonora, E., Gorini, P., Bolognesi, A., Stirpe, F., 1997. Polynucleotide: adenosine glycosidase activity of ribosome-inactivating proteins: effect on DNA, RNA and poly(A). Nucleic Acids Res. 25, 518–522.

Bolognesi, A., Barbieri, L., Abbodanza, A., Falasca, A.I., Carnicelli, D., Battelli, M.G., Stirpe, F., 1990. Purification and properties of new ribosome-inactivating proteins with RNA *N*-glycosidase activity. Biochim. Biophys. Acta 1087, 293–302.

Brünger, A.T., Kuriyan, J., Karplus, M., 1987. Crystallographic *R* factor refinement by molecular dynamics. Science 235, 458–460.

Correll, C.C., Munishkin, A., Chan, Y.L., Ren, Z., Wool, I.G., Steitz, T.A., 1998. Crystal structure of the ribosomal RNA domain essential for binding elongation factors. Proc. Natl. Acad. Sci. USA 95, 13436–13441.

Dodson, E., Kleywegt, G.J., Wilson, K., 1996. Report of a workshop on the use of statistical validators in protein X-ray crystallography. Acta Crystallogr. D 52, 228–234.

Endo, Y., Gluck, A., Wool, I.G., 1991. Ribosomal RNA identity elements for ricin A-chain recognition and catalysis. J. Mol. Biol. 221, 193–207.

Higashi, T., 1989. The processing of diffraction data taken on a screenless Weissenberg camera for macromolecular crystallography. J. Appl. Crystallogr. 22, 9–18.

Honjo, E., Dong, D., Motoshima, H., Watanabe, K., 2002. Genomic clones encoding two isoforms of pokeweed antiviral protein in seeds (PAP-S1 and S2) and the *N*-glycosidase activities of their recombinant proteins on ribosomes and DNA in comparison with other isoforms. J. Biochem. 131, 225–231.

Huang, Q., Liu, S., Tang, Y., Jin, S., Wang, Y., 1995. Studies on crystal structures, active-center geometry and depurinating mechanism of two ribosome-inactivating proteins. Biochem. J. 309, 285–298.

Hudak, K.A., Diman, J.D., Tumer, N.E., 1999. Pokeweed antiviral protein accesses ribosomes by binding to L3. J. Biol. Chem. 274, 3859–3864.

Irvin, J.D., 1975. Purification and partial characterization of the antiviral protein from *Phytolacca americana* which inhibits eukaryotic protein synthesis. Arch. Biochem. Biophys. 169, 522–528.

Irvin, J.D., Kelly, T., Robertus, J.D., 1980. Purification and properties of a second antiviral protein from *Phytolacca americana* which inactivates eukaryotic ribosomes. Arch. Biochem. Biophys. 200, 418–425.

Islam, M.R., Kung, S.S., Kimura, Y., Funatsu, G., 1991. *N*-Acetyl-D-glucosamine-asparagine structure in ribosome-inactivating proteins from the seeds of *Luffa cylindrica* and *Phytolacca americana*. Agric. Biol. Chem. 55, 1375–1381.

Jones, T.A., Zou, J.Y., Cowan, S.W., Kjeldgaard, M., 1991. Improved methods for building protein models in electron density maps and the location of errors in these models. Acta Crystallogr. A 47, 110–119.

Kataoka, J., Habuka, N., Masuta, C., Miyano, M., Koiwai, A., 1992. Isolation and analysis of a genomic clone encoding a pokeweed antiviral protein. Plant Mol. Biol. 20, 879–886.

Kleywegt, G.J., Brünger, A.T., 1996. Checking your imagination: applications of the free *R* value. Structure 4, 879–904.

Kraulis, P.J., 1991. MOLSCRIPT: a program to produce both detailed and schematic plots of protein structures. J. Appl. Crystallogr. 24, 946–950.

Kurinov, I.V., Myers, D.E., Irvin, J.D., Uckun, F.M., 1999a. X-ray crystallographic analysis of the structural basis for the interaction of pokeweed antiviral protein with its active site inhibitor and ribosomal RNA analogs. Protein Sci. 8, 1722–1765.

Kurinov, I.V., Rajamohan, T.K., Venkatachalam, T.K., Uckun, F.M., 1999b. X-ray crystallographic analysis of the structural basis for the interaction of pokeweed antiviral protein with guanine residues of ribosomal RNA. Protein Sci. 8, 2399–2405.

Laskowski, R.A., MacArthur, M.W., Moss, D.S., Thorton J.M, 1993. PROCHECK: a program to check the stereo chemical quality of protein structure. J. Appl. Crystallogr. 28, 283–291.

Li, H.M., Zeng, Z.H., Hu, Z., Wang, D.C., 1998. Crystallization and preliminary crystallographic analyses of pokeweed antiviral protein from seeds. Acta Crystallogr. D 54, 137–139.

Monzingo, A.F., Collins, E.J., Erust, S.R., Irvin, J.D., Robertus, J.D., 1993. The 2.5 Å structure of pokeweed antiviral protein. J. Mol. Biol. 233, 705–715.

Monzingo, A.F., Robertus, J.D., 1992. X-ray analysis of substrate analogs in the ricin A-chain active site. J. Mol. Biol. 227, 1136–1145.

Navaza, J., 1994. AmoRe—an automated package for molecular replacement. Acta Crystallogr. A 50, 157–163.

Nicholls, A.J., 1993. GRASP Manual. Columbia University.

Otwinowski, Z., Minor, W., 1997. In: Carter Jr., C.W., Sweet, R.M. (Eds.), Processing of X-ray diffraction Data Collected in Oscillation Mode. Methods in Enzymology, vol. 276, part A. Academic Press, New York, pp. 307–326.

Ramachandran, G.N., Sasusekharan, V., 1968. Conformation of polypeptide and protein. Advan. Protein. Chem. 23, 283–437.

Roussel, A., Cambillau, C., 1991. TURBO-FRODO in Silicon Grasphics Geometry Partners Directory 86. Silicon Graphics, Mountain View, CA, USA.

Sakabe, N., 1989. A focusing Weissenburg camera with multi-layer-line screens for macromolecular crystallography. J. Appl. Crystallog. 16, 542–547.

Stirpe, F., Barbieri, L., Battelli, M.G., Soria, M., Lappi, D.A., 1992. Ribosome-inactivating proteins from plants: present status and future prospects. Biotechnology 10, 405–412.

Wang, Y.X., Neamati, N., Jacob, J., Palmer, I., Stahl, S., Kaufman, J.D., Huang, P.L., Huang, P.L., Winslow, H.E., Pommier, Y., Wingfield, P.T., Lee-Huang, S., Bax, A., Torchia, D.A., 1999. Solution structure of anti-HIV-1 and antitumor protein MAP30: structural insights into its multiple functions. Cell 99, 433–442.

Wormald, M.R., Dwek, R.A., 1999. Glycoproteins: glycan presentation and protein-fold stability. Structure 7, R155–R160.

Zhu, X., Hu, Z., 1989. Preparation of the antiviral protein from pokeweed seeds and assay of its toxicity. Acta Bot. Yunnanica 11, 440–448.